
AN ASYNCHRONOUS KALMAN FILTER FOR HYBRID EVENT CAMERAS

PREPRINT*

 **Ziwei Wang**

Systems Theory and Robotics Group
Australian National University
ACT, 2601, Australia
ziwei.wang1@anu.edu.au

 **Yonhon Ng**

Systems Theory and Robotics Group
Australian National University
ACT, 2601, Australia
yonhon.ng@anu.edu.au

 **Cedric Scheerlinck**

Systems Theory and Robotics Group
Australian National University
ACT, 2601, Australia
cedric.scheerlinck@anu.edu.au

 **Robert Mahony**

Systems Theory and Robotics Group
Australian National University
ACT, 2601, Australia
robert.mahony@anu.edu.au

July 13, 2021

ABSTRACT

We present an Asynchronous Kalman Filter (AKF) to reconstruct High Dynamic Range (HDR) videos by fusing low-dynamic range images with event data. Event cameras are ideally suited to capture HDR visual information without blur but perform poorly on static or slowly changing scenes. Conversely, conventional image sensors measure absolute intensity of slowly changing scenes effectively but do poorly on quickly changing scenes with high dynamic range. The proposed approach exploits advantages of hybrid sensors under a unifying uncertainty model for both conventional frames and events. We present a novel dataset targeting challenging HDR and fast motion scenes captured on two separate sensors: an RGB frame-based camera and an event camera. Our video reconstruction outperforms the state-of-the-art algorithms on existing datasets and our targeted HDR dataset.

Code, Datasets and Video:

<https://github.com/ziweiWWANG/AKF>

1 Introduction

Event cameras offer distinct advantages over conventional frame-based cameras: high temporal resolution, high dynamic range (HDR) and minimal motion blur [19]. However, event cameras provide poor imaging capability in slowly varying or static scenes, where despite some efforts in ‘gray-level’ event cameras that measure absolute intensity [30, 5], most sensors predominantly measure only the relative intensity change. Conventional imaging technology, conversely, is ideally suited to imaging static scenes and measuring absolute intensity. Hybrid sensors such as the Dynamic and Active Pixel Vision Sensor (DAVIS) [3] or custom-built systems [43] combine event and frame-based cameras, and there is an established literature in video reconstruction fusing conventional and event camera data. The potential of such algorithms to enhance conventional video to overcome motion blur and increase dynamic range has applications from robotic vision systems (*e.g.*, autonomous driving), through film-making to smartphone applications for everyday use.

Event cameras respond to local changes in brightness rather than absolute brightness levels. They inherently have high intra-scene dynamic range since the relative change in irradiance is measured pixel-by-pixel as a ratio yielding log-sensitivity. Changes in irradiance trigger ‘events’ that are asynchronously measured with microsecond precision. The minimum brightness change required to trigger an event is called the contrast threshold and this acts as a log-scale quantisation of relative intensity as measured by a given event camera. Blur artifacts caused by motion during exposure of a conventional camera sensor are not present in event data since there is no exposure time, although extremely fast motions can result in erroneous and missed events.

*Under review

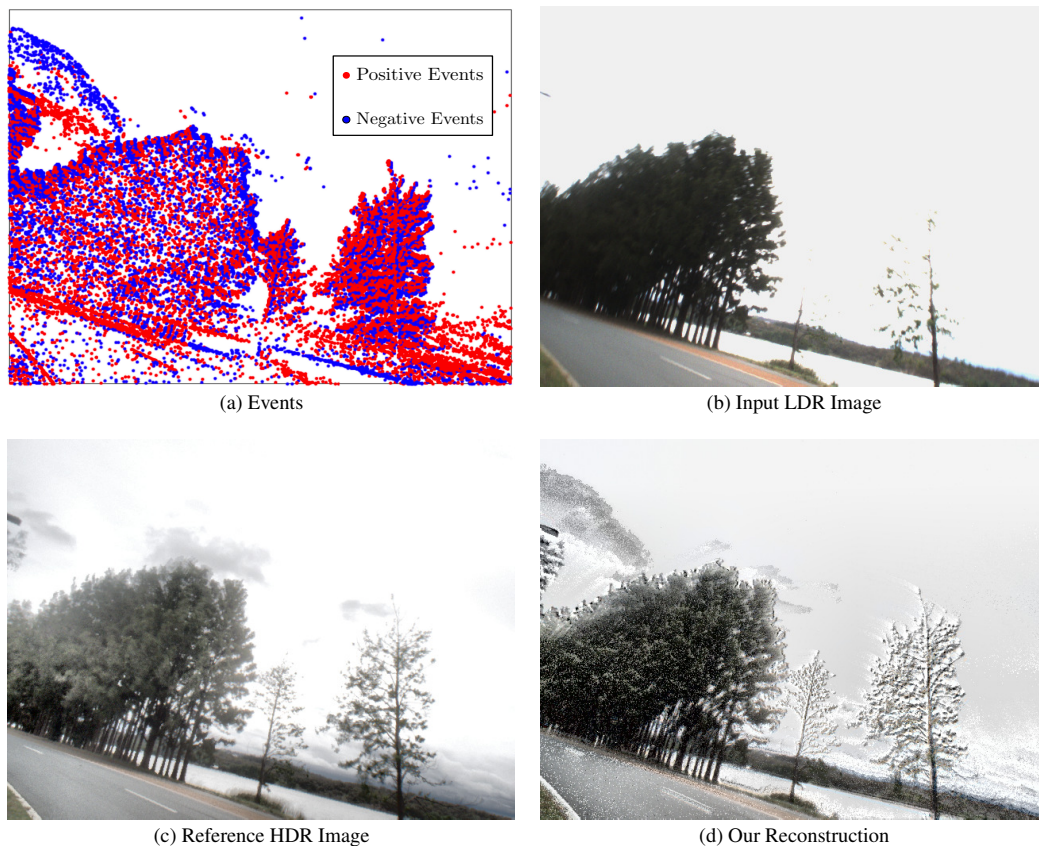


Figure 1: An example from our new hybrid event/frame HDR dataset. Events (a), and low dynamic range video (b), from a hybrid event/frame camera sensor, are fused to generate a high frame-rate high dynamic-range video (d). The reference HDR image (c) is obtained by fusing multiple images at different exposures.

In this paper, we propose an asynchronous Kalman Filter (AKF) to reconstruct high-speed, HDR video from hybrid event/frame cameras. Unlike previous works on temporal filtering for event cameras [36, 37] that use constant gain, this paper introduces an explicit noise model for both events and frames that is used in a Kalman filter framework. Our algorithm maintains asynchronous filter states for the output video as well as noise covariance states that are used to update the Kalman gain. We propose a novel temporal interpolation scheme that we apply to input frames in addition to de-blurring [27] as a preprocessing step called *frame augmentation*.

To evaluate the proposed pipeline, we present a novel HDR hybrid event/frame dataset. The DAVIS event camera, popular in existing datasets, suffers from ‘shutter noise’, which are triggered with every frame readout due to undesirable capacitive coupling in pixel circuitry [3]. DAVIS frames are relatively low resolution, low dynamic range and low framerate. To overcome these limitations, we built a hybrid system consisting of an RGB frame-based camera mounted alongside an event camera to collect events, frames and HDR groundtruth. In summary, our contributions are:

- An asynchronous Kalman filter (AKF) for hybrid event/frame HDR video reconstruction
- A unifying event/frame uncertainty model
- Deblur and temporal interpolation for frame augmentation
- A novel real-world HDR hybrid event/frame dataset.

2 Related Work

Hybrid event/frame cameras such as the DAVIS [3] were developed shortly after pure event cameras (DVS) [19], recognising the limited ability of event cameras to detect slow/static scenes and absolute brightness. Image frames are captured on the same chip and through the same lens allowing the two complementary data streams to be exactly registered [4]. This has led to significant research effort into image reconstruction from hybrid event/frame and pure event cameras including SLAM-based methods [6, 17, 31], filters [36, 37], de-blurring [26, 27], super-resolution and machine learning approaches [33, 38, 41].

While batch methods have achieved high accuracy, they incur additional latency depending on the time-interval of the batch (*e.g.*, 50ms). Asynchronous methods, if implemented on appropriate hardware, have the potential to run on a timescale closer to that of events $< 1\text{ms}$. A further distinction may be made between pure event reconstruction methods and hybrid event/frame methods that use a mix of (registered) events and image frames. Our approach falls into the hybrid event/frame category and relies on a small buffer of events, though most of the computation runs asynchronously.

Pure event reconstruction:

Images and video reconstruction using only events is a topic of significant interest in the community that can shed light on the information content of events alone. Early works focused on mapping static scenes while tracking a moving event camera, either pure rotations [6, 16] or full 6-DOF motion [17, 31]. Hand-crafted approaches were proposed including joint optimisation over optic flow and image intensity [1], periodic regularisation based on event timestamps [34] and temporal filtering [36, 37]. Recently, learned approaches have achieved surprisingly high quality video reconstruction [32, 33, 38, 41] at significantly higher computational cost vs. hand-crafted methods.

Event-frame reconstruction:

The invention of the DAVIS [3] and its ability to capture frames alongside events (and even IMU measurements) has widened the community’s perspective from pure event cameras to hybrid sensors and how best to combine modalities. A simple approach is to start from an image and add events scaled by the contrast threshold [4]. The contrast threshold is typically unknown and variable, so [4] propose a simple method to estimate it based on surrounding image frames from the DAVIS. Pan *et al.* [26, 27] devised the event double integral (EDI) relation between events and a blurry image, along with an optimisation approach to estimate contrast thresholds to reconstruct high-speed de-blurred video from events and frames. High-speed video can also be obtained by warping still images according to motion computed via events [39, 21], or by letting a neural network learn how to combine frames and events [29, 44, 28, 20, 13]. Recognising the limited spatial resolution of the DAVIS, Wang *et al.* [43] built a hybrid sensor consisting of an RGB camera and a DAVIS240 event camera registered via a beam-splitter. They proposed guided event filtering to fuse frame and event information from their hybrid sensor.

Continuous-time temporal filtering is an approach that exploits the near-continuous nature of events. Scheerlinck *et al.* [36, 37] proposed an asynchronous complementary filter to fuse events and frames that can equivalently be run as a high-pass filter if the frame input is set to zero (*i.e.*, using events only). The filters are based on temporal smoothing via a single fixed-gain parameter that determines the ‘fade rate’ of the event signal. Our method dynamically adjusts per-pixel gains according to our proposed uncertainty model based on Kalman-Bucy filtering [14, 15].

3 Sensor Model and Uncertainty

3.1 Event Camera Model

Event cameras measure the relative log intensity change of irradiance of pixels. New events $e_{\vec{p}}^i$ are triggered when the log intensity change exceeds a preset contrast threshold c . In this work, we model events as a Dirac delta function to allow us to apply continuous time systems analysis for filter design. That is,

$$e_{\vec{p}}(t) = \sum_{i=1}^{\infty} (c\sigma_{\vec{p}}^i + \eta_{\vec{p}}^i) \delta(t - t_{\vec{p}}^i), \quad (1)$$

$$\eta_{\vec{p}}^i \sim \mathcal{N}(0, Q_{\vec{p}}(t)),$$

where $t_{\vec{p}}^i$ is the time of the i^{th} event at the $\vec{p} = (\vec{p}_x, \vec{p}_y)^T$ pixel coordinate, the polarity $\sigma_{\vec{p}}^i \in \{-1, +1\}$ represents the direction of the log intensity change and the noise $\eta_{\vec{p}}^i$ is an additive Gaussian uncertainty at the instance when the event occurs. The noise covariance $Q_{\vec{p}}(t)$ is the sum of three contributing noises modelled by ‘process’, ‘isolated pixel’, and ‘refractory period’ which is

$$Q_{\vec{p}}(t) := \sum_{i=1}^{\infty} \left(Q_{\vec{p}}^{\text{proc.}}(t) + Q_{\vec{p}}^{\text{iso.}}(t) + Q_{\vec{p}}^{\text{ref.}}(t) \right) \delta(t - t_{\vec{p}}^i). \quad (2)$$

We further discuss the three noises in the next section.

3.1.1 Event Camera Uncertainty

Stochastic models for event camera uncertainty are difficult to develop and justify [9]. In this paper, we propose a number of simple heuristics to model event noise as the sum of three pixel-by-pixel additive Gaussian processes.

Process noise:

Process noise is a constant additive uncertainty in the evolution of the irradiance of the pixel, analogous to process noise in a Kalman filtering model. Since this noise is realised as an additive uncertainty only when an event occurs, we call on the principles of Brownian motion to model the uncertainty at time $t_{\vec{p}}^i$ as a Gaussian process with covariance that grows linearly with time since the last event at the same pixel. That is

$$Q_{\vec{p}}^{\text{proc.}}(t_{\vec{p}}^i) = \sigma_{\text{proc.}}^2 (t_{\vec{p}}^i - t_{\vec{p}}^{i-1}),$$

where $\sigma_{\text{proc.}}^2$ is a tuning parameter associated with the process noise level.

Isolated pixel noise:

Spatially and temporally isolated events are more likely to be associated to noise than events that are correlated in group. The noisy background activity filter [8] is designed to suppress such noise and most events cameras have similar routines that can be activated. Instead, we model an associated noise covariance by

$$Q_{\vec{p}}^{\text{iso.}}(t_{\vec{p}}^i) = \sigma_{\text{iso.}}^2 \min\{t_{\vec{p}}^i - t_{N(\vec{p})}^*\},$$

where $\sigma_{\text{iso.}}^2$ is a tuning parameter and $t_{N(\vec{p})}^*$ is the latest time-stamp of any event in a neighbourhood $N(\vec{p})$ of \vec{p} . If there are recent spatio-temporally correlated events then $Q_{\vec{p}}^{\text{iso.}}(t_{\vec{p}}^i)$ is negligible, however, the covariance grows linearly, similar to the Brownian motion assumption for the process noise, with time from the most recent event.

Refractory period noise:

Circuit limitations in each pixel of an event camera limit the response time of events to a minimum known as the refractory period $\rho > 0$ [45]. If the event camera experience fast motion in highly textured scenes then the pixel will not be able to trigger fast enough and events will be lost. We model this by introducing a dependence on the uncertainty associated with events that are temporally correlated such that

$$Q_{\vec{p}}^{\text{ref.}}(t_{\vec{p}}^i) = \begin{cases} 0 & \text{if } t_{\vec{p}}^i - t_{\vec{p}}^{i-1} > \bar{\rho} \\ \sigma_{\text{ref.}}^2 & \text{if } t_{\vec{p}}^i - t_{\vec{p}}^{i-1} \leq \bar{\rho}, \end{cases}$$

where $\sigma_{\text{ref.}}^2$ is a tuning parameter and $\bar{\rho}$ is an upper bound on the refractory period.

3.2 Conventional Camera Model

The photo-receptor in a CCD or CMOS circuit from a conventional camera converts incoming photons into charge that is then converted to a pixel intensity by an analogue-to-digital converter (ADC). In a typical camera the sensor irradiance is linearly related to the charge generated for the correct choice of exposure, but can become highly non-linear where pixels are over-exposed or under-exposed [22]. Effects such as dark current noise and CCD saturation and blooming further destroy the linearity of the camera response at the extreme intensities [18]. The mapping of sensor irradiance to the sensor response is termed the Camera Response Function (CRF) [10]. The CRF can be estimated using an image sequence taken under different exposures [7, 23, 10]. For long exposures pixels that would have been correctly exposed become over exposed and provide information on the nonlinearity of the CRF at high intensity, and similarly for short exposures and the low intensity part of the CRF. We have used this approach to estimate the CRF for the APS sensor on a DAVIS event camera and a FLIR camera that we use for our experimental data Fig. 2.

In a digital camera, the sensor response is quantised and then scaled through the inverse of the CRF to produce the digitised raw intensity output

$$I_{\vec{p}}^F(\tau^k) = CRF^{-1}[\lfloor I_{\vec{p}}(\tau^k) \rfloor] + \mu_{\vec{p}}^k, \quad (3)$$

$$\mu_{\vec{p}}^k \sim N(0, \bar{R}_{\vec{p}}(\tau^k)),$$

where $I_{\vec{p}}^F(\tau^k)$ is the digital output and $\lfloor I_{\vec{p}}(\tau^k) \rfloor$ is the quantization of the nominal sensor response $I_{\vec{p}}(\tau^k)$. The noise parameters for $\mu_{\vec{p}}^k$ are principally derived from the quantisation process and can be related to the camera response function as discussed below. The timestamp τ^k for the frame is global.

3.2.1 Conventional Camera Uncertainty

Both uncertainty in the sensor response $I_{\vec{p}}(\tau^k)$ and the additional quantisation noise are mapped through the inverse of the CRF to result in noise in the raw intensity output $I_{\vec{p}}^F(\tau^k)$. The sensor response noise is usually modelled as a constant variance Gaussian process [40, 35], and quantisation noise is linear in the sensor response. It follows that the dominant effect in modelling camera frame noise for extreme exposures is associated with inverting the camera response function [22, 10, 18].

The CRF is experimentally determined as a function of exposure E by correlating a constant irradiance scene over multiple exposures [7, 23, 10] (Fig 2.a). The certainty function is defined to be the sensitivity, $dCRF/dE$, of the CRF with respect to

exposure (Fig 2.b) [10]. Note that different cameras can have dissimilar responses to exposure time for the same irradiance of the sensor. Re-scaling the exposure axis to raw intensity and renormalising (so that the maximum is unity) the associated certainty defines the weighting function (Fig 2.c) as a function of raw image intensity [10]. We propose to model the covariance of noise associated with raw image intensity as the scaled inverse of the weighting function for a given camera (Fig 2.d). That is, we define

$$\bar{R}_{\vec{p}}(\tau^k) := \sigma_{\text{im.}}^2 \frac{dI_{\vec{p}}^F/dE}{d\text{CRF}/dE}, \quad (4)$$

where $\sigma_{\text{im.}}^2$ is a tuning parameter related to the base level of noise in the image and $dI_{\vec{p}}^F/dE$ is an affine relationship associating exposure time to raw image intensity (see Figure 2.d. for $\sigma_{\text{im.}}^2 = 1$). Note that we also introduce a saturation to assign a maximum value to the covariance (Fig. 2.d).

In addition to the base uncertainty model for raw image intensity we will also need to model uncertainty of image frames in the interframe period and in the log intensity scale for the proposed algorithm. We use linear interpolation to extend the covariance estimate from two consecutive frames $I_{\vec{p}}^F(\tau^k)$ and $I_{\vec{p}}^F(\tau^{k+1})$ by

$$\bar{R}_{\vec{p}}(t) := \left(\frac{t - \tau^k}{\tau^{k+1} - \tau^k} \right) \bar{R}_{\vec{p}}(\tau^{k+1}) + \left(\frac{\tau^{k+1} - t}{\tau^{k+1} - \tau^k} \right) \bar{R}_{\vec{p}}(\tau^k). \quad (5)$$

We define the continuous log image intensity function by taking the log of $I_{\vec{p}}^F$. However, since the log function is not symmetric and mapping the noise on $I_{\vec{p}}^F$ will bias the log intensity. To compensate for this bias we define

$$L_{\vec{p}}^F(\tau^k) := \log(I_{\vec{p}}^F(\tau^k) + I_0) - \frac{\bar{R}_{\vec{p}}(\tau^k)}{2(I_{\vec{p}}^F(\tau^k) + I_0)^2} + \mu_{\vec{p}}^k, \quad (6)$$

$$\mu_{\vec{p}}^k \sim \mathcal{N}(0, R_{\vec{p}}(\tau^k))$$

where I_0 is a fixed offset introduced to ensure intensity values remain positive and $R_{\vec{p}}(\tau^k)$ is the covariance of noise associated with the log intensity. The covariance is given by

$$R_{\vec{p}}(t) = \frac{\bar{R}_{\vec{p}}(t)}{2(I_{\vec{p}}^F(\tau^k) + I_0)^2}. \quad (7)$$

Generally, when the raw intensity is not extreme then $\frac{\bar{R}_{\vec{p}}(t)}{2(I_{\vec{p}}^F(\tau^k) + I_0)^2} \ll \log(I_{\vec{p}}^F(\tau^k) + I_0)$ and $L_{\vec{p}}^F(\tau^k) \approx \log(I_{\vec{p}}^F(\tau^k) + I_0)$.

4 Method

The proposed image processing architecture is shown in Figure 3. There are three modules in the proposed algorithm; a frame augmentation module that uses events to augment the raw frame data to remove blur and increase temporal resolution, the Kalman gain module that integrates the uncertainty models to compute the filter gain, and the Asynchronous Kalman Filter that fuses the augmented frame data with the event stream to generate HDR video.

4.1 Frame Augmentation

Deblur:

Due to long exposure time or fast motion, the intensity images L^F may suffer from severe motion blur. We use the double integral model (EDI) from [27] to sharpen the blurry low frequency images to obtain a deblurred image $L_{\vec{p}}^D(\tau^k - T/2)$ at the beginning, and $L_{\vec{p}}^D(\tau^{k+1} + T/2)$ at the end, of the exposure of each frame (Fig. 4). The two sharpened images are used in the interpolation module.

Interpolation:

The goal of the interpolation module is to increase the temporal resolution of the frame data. This is important to temporally align the information in the image frame and event streams of data, which helps overcome the ghosting effects that are visible in other recent work where the image frames are interpolated using zero order hold [36, 37].

To estimate intensity at the i^{th} event timestamp at pixel \vec{p} we integrate forward from a deblurred image $L_{\vec{p}}^D(\tau^k - T/2)$ taken from the start of the exposure (Fig. 4). That is the forward interpolation is

$$L_{\vec{p}}^{A-}(t) = L_{\vec{p}}^D(\tau^k - T/2) + \int_{\tau^k - T/2}^t c_{\vec{p}}^k e(\gamma) d\gamma. \quad (8)$$

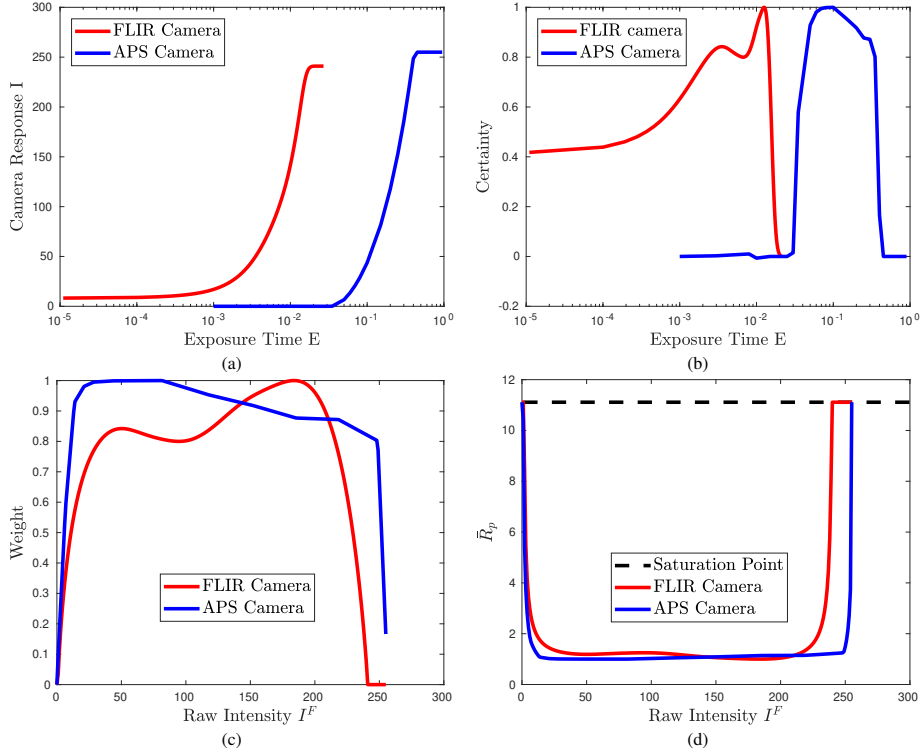


Figure 2: Camera functions for the APS camera in a DAVIS event/frame camera (blue) and the FLIR camera (red) used in the experimental studies.

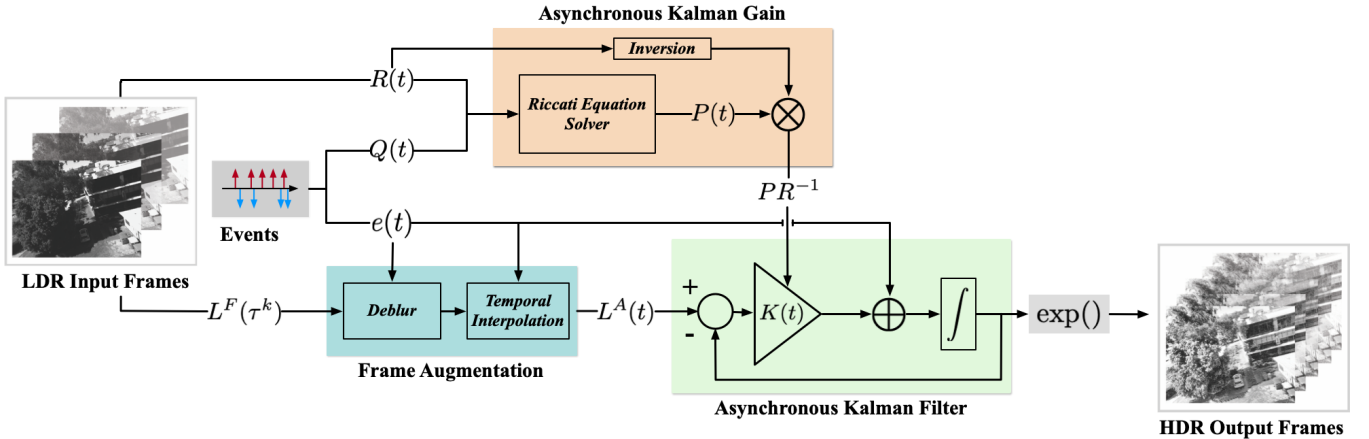


Figure 3: Block diagram of the image processing pipeline discussed in Method §4.

where $L_{\bar{p}}^{A-}$ denotes the augmented image. Similarly, we interpolate backwards from the end of exposure $k + 1$ to obtain

$$L_{\bar{p}}^{A+}(t) = L_{\bar{p}}^D(\tau^{k+1} + T/2) - \int_t^{\tau^{k+1} + T/2} c_{\bar{p}}^k e(\gamma) d\gamma, \quad (9)$$

where $c_{\bar{p}}^k$ is a variable per-pixel contrast threshold that we discuss below.

Ideally, if there are no missing or biased events and the frame data is not noisy, then the forwards and backwards interpolation results $L_{\bar{p}}^{A-}(t_{\bar{p}}^i)$ and $L_{\bar{p}}^{A+}(t_{\bar{p}}^i)$ computed with the true contrast threshold should be equal. However, noise in either the event stream or in the frame data will cause the two interpolations to differ. We reconcile these two estimates by per-pixel calibration of the contrast threshold in each interpolation period. Define

$$c_{\bar{p}}^k := \frac{L_{\bar{p}}^D(\tau^{k+1} + T/2) - L_{\bar{p}}^D(\tau^k - T/2)}{\int_{\tau^k}^{\tau^{k+1}} e(\gamma) d\gamma}. \quad (10)$$

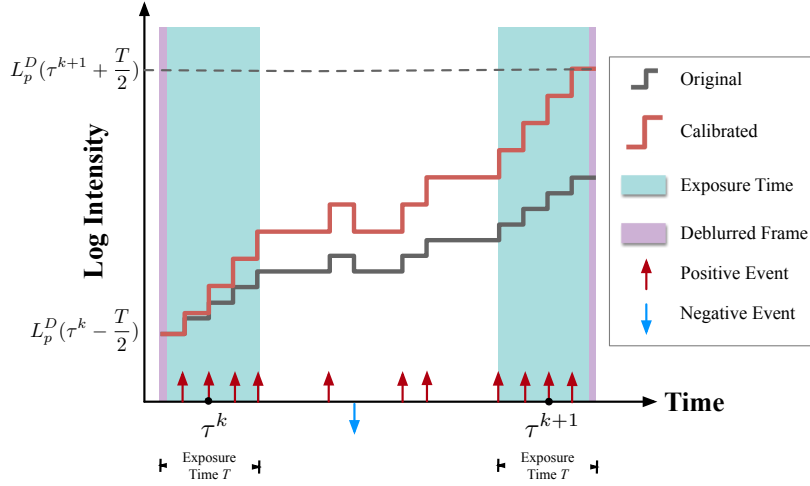


Figure 4: Frame augmentation. Two deblurred frames at times $\tau^k - \frac{T}{2}$ and $\tau^{k+1} + \frac{T}{2}$ are computed. The event stream is used to interpolate between the two deblurred frames to improve temporal resolution.

This calibration can be seen as using the shape provided by the event integration between deblurred frames and changing the contrast threshold to vertically stretch or shrink the interpolation to fit the deblurred frame data (Fig. 4). This is particularly effective at compensating for refractory noise where missing events are temporally correlated to the remaining events. Using the outer limits of the exposure for the deblurred image maximises the number of events (per-pixel) in the interpolation period and improves the estimation of $c_{\bar{p}}^k$.

Within each exposure (frame k) there is a forward and backward estimate available with different per-pixel contrast thresholds associated with interpolating from frame $k - 1$ to frame k and from frame k to frame $k + 1$. We smoothly interpolate between estimates in the exposure period to define the final augmented frame

$$L_{\bar{p}}^A(t) = \begin{cases} \left(\frac{t - \tau^k - T/2}{T} \right) L_{\bar{p}}^{A+}(t) + \left(\frac{\tau^k + T/2 - t}{T} \right) L_{\bar{p}}^{A-}(t), & \text{if } t \in [\tau^k - T/2, \tau^k + T/2) \\ L_{\bar{p}}^{A+}(t), & \text{if } t \in [\tau^k + T/2, \tau^{k+1} - T/2). \end{cases} \quad (11)$$

4.2 Asynchronous Kalman Filter (AKF)

The approach taken is to consider the continuous time stochastic model.

$$\begin{aligned} dL_{\bar{p}} &= e_{\bar{p}}(t)dt + dw_{\bar{p}}, \\ L_{\bar{p}}^A(t_{\bar{p}}^i) &= L_{\bar{p}}(t_{\bar{p}}^i) + \mu_{\bar{p}}^i, \end{aligned}$$

where $dw_{\bar{p}}$ is a Wiener process and $\mu_{\bar{p}}^i$ is the log intensity frame noise (6). Since the event stream is a sum of dirac-delta functions, the continuous integral decomposes into an asynchronous sum of event updates

$$L_{\bar{p}}(t_{\bar{p}}^{i+}) = L_{\bar{p}}(t_{\bar{p}}^{i-}) + e_{\bar{p}}(t_{\bar{p}}^i) + \eta_{\bar{p}}^i, \quad (12)$$

where $\eta_{\bar{p}}^i$ is the event noise (1). The Kalman-Bucy filter that we implement is posed in continuous-time and implemented asynchronously as each event arrives. The nominal model that we consider is

$$\dot{\hat{L}}_{\bar{p}}(t) = e_{\bar{p}}(t) - K_{\bar{p}}(t)[\hat{L}_{\bar{p}}(t) - L_{\bar{p}}^A(t)] \quad (13)$$

However, we solve this ordinary differential equation in a series of time intervals $t \in [t_{\bar{p}}^i, t_{\bar{p}}^{i+1})$ as a discrete update based on (12), followed by solving (13). That is

$$L_{\bar{p}}(t_{\bar{p}}^i) = \hat{L}_{\bar{p}}(t_{\bar{p}}^{i-}) + e_{\bar{p}}(t_{\bar{p}}^i) \quad (14)$$

$$\dot{\hat{L}}_{\bar{p}}(t) = -K_{\bar{p}}(t)[\hat{L}_{\bar{p}}(t) - L_{\bar{p}}^A(t)] \quad \text{for } t \in [t_{\bar{p}}^i, t_{\bar{p}}^{i+1}), \quad (15)$$

where $\hat{L}^A(t)$ is the augmented image (11).

Metrics	MSE ($\times 10^{-2}$) ↓				SSIM ↑				Q score ↑			
Methods	E2VID	ECNN	CF	AKF (ours)	E2VID	ECNN	CF	AKF (ours)	E2VID	ECNN	CF	AKF (ours)
Dataset	HDR sequences											
City	2.02	1.60	3.40	0.33	0.61	0.47	0.44	0.87	3.99	2.42	3.74	5.40
Trees 1	2.45	5.73	8.07	1.79	0.73	0.53	0.53	0.82	4.54	4.26	2.85	5.44
Trees 2	9.96	16.28	5.83	0.85	0.54	0.11	0.83	0.97	4.50	3.32	3.88	5.18
Trees 3	22.48	26.84	8.38	4.79	0.41	0.15	0.78	0.86	4.52	3.19	3.03	4.77
Building	1.91	6.71	5.41	0.81	0.79	0.30	0.74	0.94	4.05	3.86	1.54	3.36
Mean	7.76	11.43	6.22	1.71	0.616	0.31	0.66	0.89	4.32	3.41	3.01	4.83
Dataset	Artificial HDR sequences (AHDR)											
Mountain slow	17.19	33.03	7.43	6.49	0.53	-0.14	0.57	0.71	5.36	2.83	5.19	5.87
Mountain fast	17.75	36.69	7.87	6.47	0.56	-0.23	0.52	0.70	5.34	2.76	4.47	5.19
Lake slow	4.83	7.99	2.72	1.81	0.48	0.22	0.70	0.80	5.18	3.82	5.01	5.76
Lake fast	6.47	7.21	3.11	1.93	0.43	0.30	0.70	0.80	5.07	4.01	4.45	5.35
Mean	11.56	21.23	5.28	4.18	0.50	0.04	0.62	0.75	5.24	3.36	4.78	5.54

Table 1: Comparison of the state-of-the-art (SoTA) methods of event-based video reconstruction on our HDR dataset. Our AKF consistently outperforms SoTA on all metrics. AHDR sequences generated by restricting dynamic range of input images.

Metrics	MSE ($\times 10^{-2}$) ↓				SSIM ↑				LPIPS ↓			
Methods	E2VID	ECNN	CF	AKF (ours)	E2VID	ECNN	CF	AKF (ours)	E2VID	ECNN	CF	AKF (ours)
Mean	20.67	6.41	0.21	0.18	0.43	0.56	0.85	0.86	0.37	0.24	0.19	0.19

Table 2: Mean results on IJRR [24] DAVIS event camera dataset.

An analytic form for the time-evolution of the Kalman gain $K_{\bar{p}}(t) = P_{\bar{p}}(t)R_{\bar{p}}^{-1}(t)$ is given by (18). Using this, we can derive an analytic solution for (15) (see Appendix)

$$\hat{L}_{\bar{p}}(t) = \frac{[\hat{L}_{\bar{p}}(t_{\bar{p}}^i) - L_{\bar{p}}^A(t_{\bar{p}}^i)] \cdot P_{\bar{p}}^{-1}(t_{\bar{p}}^i)}{P_{\bar{p}}^{-1}(t_{\bar{p}}^i) + R_{\bar{p}}^{-1}(t) \cdot (t - t_{\bar{p}}^i)} + L_{\bar{p}}^A(t). \quad (16)$$

4.3 Asynchronous Kalman Gain

Let $P_{\bar{p}}(t) > 0$ denote the variance of the state estimate in the Kalman-Bucy filter. The Riccati equation that governs the evolution of the state variance is given by

$$\dot{P}_{\bar{p}} = -P_{\bar{p}}^2 R_{\bar{p}}(t) + Q_{\bar{p}}(t),$$

where $R_{\bar{p}}(t)$ (7) is the log-intensity frame covariance and $Q_{\bar{p}}(t)$ (2) is the event noise covariance. Here the choice of process noise model (2) as a discrete noise that occurs when the update of information occurs means that the Riccati equation can also be solved as an asynchronous update with an analytic solution of

$$\dot{P}_{\bar{p}}(t) = -P_{\bar{p}}^2(t) \cdot R_{\bar{p}}^{-1}(t), \quad (17)$$

on the time interval $t \in [t_{\bar{p}}^i, t_{\bar{p}}^{i+1})$. Since $R_{\bar{p}}(t)$ is constant on this time interval then the solution of (17) is (see Appendix)

$$P_{\bar{p}}(t) = \frac{1}{P_{\bar{p}}^{-1}(t_{\bar{p}}^i) + R_{\bar{p}}^{-1}(t) \cdot (t - t_{\bar{p}}^i)}, \quad \text{for } t \in [t_{\bar{p}}^i, t_{\bar{p}}^{i+1}). \quad (18)$$

The reset at time $t_{\bar{p}}^{i-}$ is given by

$$P_{\bar{p}}(t_{\bar{p}}^i) = P_{\bar{p}}(t_{\bar{p}}^{i-}) + Q_{\bar{p}}(t_{\bar{p}}^i). \quad (19)$$

The Kalman gain is given by

$$K_{\bar{p}}(t) = P_{\bar{p}}(t)R_{\bar{p}}^{-1}(t).$$

5 Hybrid Event/Frame Dataset

Evaluating HDR reconstruction for hybrid event/frame cameras requires a dataset including synchronised events, low dynamics range video and high dynamic range reference images. The dataset associated with the recent work by [11] is patent protected and not publicly available. Published datasets lack high quality HDR reference images, instead relying on low dynamic range sensors such as the APS component of a DAVIS for groundtruth [41, 48, 24] and do not target HDR scenes [43]. DAVIS cameras also incur shutter noise (noise events triggered by APS frame readout) due to undesirable coupling between APS and DVS components of pixel circuitry [3]. To address these limitations, we built a hybrid event/frame camera system consisting of two separate high quality sensors, a Prophesee event camera (VGA, 640×480 pixels) and a FLIR RGB frame camera (Chameleon3 USB3, 2048×1536 pixels, 55FPS, lens of 4.5mm/F1.95), mounted side-by-side. We calibrated the hybrid system using a blinking checkerboard video and computed camera intrinsic and extrinsic matrices following [12, 47]. We synchronized the two cameras by sending an external signal from the frame camera to trigger timestamped zero magnitude events in the event camera.

The principle behind generating HDR reference images is to fuse several registered low dynamic range (LDR) images of various exposures that sample different sections of the full intensity range. This method only permits static scenes and incurs errors if there are moving components (*e.g.*, clouds), so care was taken to capture scenes in still conditions. The hybrid event/frame data was acquired separately to HDR reference images and registered in post-processing via SURF feature matching [2]. We chose long range (outdoor), static scenes to minimise disparity and registration error between frame and event camera and simplify the generation of HDR reference images.

We also provide an artificial HDR data which was generated by simulating a low dynamic range (LDR) camera by applying an artificial camera response function to real images and using the original images as HDR references. We synthesised LDR images in this manner to provide additional data to verify the performance of our algorithm.

6 Experiments

We compared our proposed Asynchronous Kalman Filter (AKF) with the state-of-the-art event-based video reconstruction methods on our novel HDR dataset and the event camera dataset (IJRR) [24]. E2VID [33] and ECNN [41] are neural networks that use only events to reconstruct video, while CF [36] combine events and frames.

Evaluation:

We evaluated image reconstruction quality using the following metrics: the structural similarity (SSIM) [42] and the learned perceptual image patch similarity (LPIPS) [46]. The Q-score [25] is a metric tailored to HDR full-reference evaluation that we additionally compute for our HDR dataset. All metrics are computed on the un-altered reconstruction and raw HDR intensities. For the IJRR dataset, we skip every second image frame as input for the algorithm and then evaluate on the intermediate frame in order that the algorithm has not ‘seen’ the ground truth data.

Main Results:

The settings for our AKF are as follows. The frame noise covariance $R_p(t)$ (7) is initialised to the median of the frame camera log intensity range and the event noise covariance $Q_{\bar{p}}$ (2) is initialised to 0.01. The tuning parameter σ_{im}^2 (4) is set to 7×10^7 for the FLIR camera and 7×10^5 for the DAVIS240C camera to account for higher relative confidence associated with the intensity value of the FLIR camera. The event noise covariance tuning parameters (2) are set to: $\sigma_{ref}^2 = 0.01$, $\sigma_{proc}^2 = 0.0005$ and $\sigma_{iso}^2 = 0.03$.

Table 1 shows that our AKF outperforms the state-of-the-art on our HDR dataset on MSE, SSIM and Q-score. Unsurprisingly, our AKF outperforms E2VID and ECNN since it utilises frame information in addition to events. Interestingly, there are rare cases where E2VID is best on Q-score, however, when taking into account all quality metrics, our method AKF is best, illustrating the importance of measuring several metrics. CF actually underperforms E2VID and ECNN in some cases despite utilising frame information in addition to events. AKF performance demonstrates the importance of taking into account frame and event noise and preprocessing frame inputs compared to CF.

Figure 5 shows qualitative samples of input, reconstructed and reference images from our HDR dataset. To improve visualisation of HDR images, we applied tonemapping using logarithmic base \log_2 and removed outliers (*i.e.*, very small or large values) before normalize image to $[0, 1]$. Then we increase image contrast using adaptive histogram equalization (CLAHE).

The event camera dataset (IJRR) [24] is a popular dataset used in several event-based video reconstruction works and though it is not targeted at HDR data, we include it here for completeness. Table 5 shows that for MSE and SSIM, AKF is almost always best, though CF is roughly equal on LPIPS. We believe the reduced gap in performance between CF and AKF is due to ‘cleaner’ frame data that is not under/overexposed as in our HDR dataset. The large difference in MSE between AKF and E2VID/ECNN is not apparent in SSIM and LPIPS, following the expectation that pure event reconstruction methods are more faithful to scene structure (captured in the latter metrics) than absolute intensity. See qualitative samples from IJRR in Appendix.

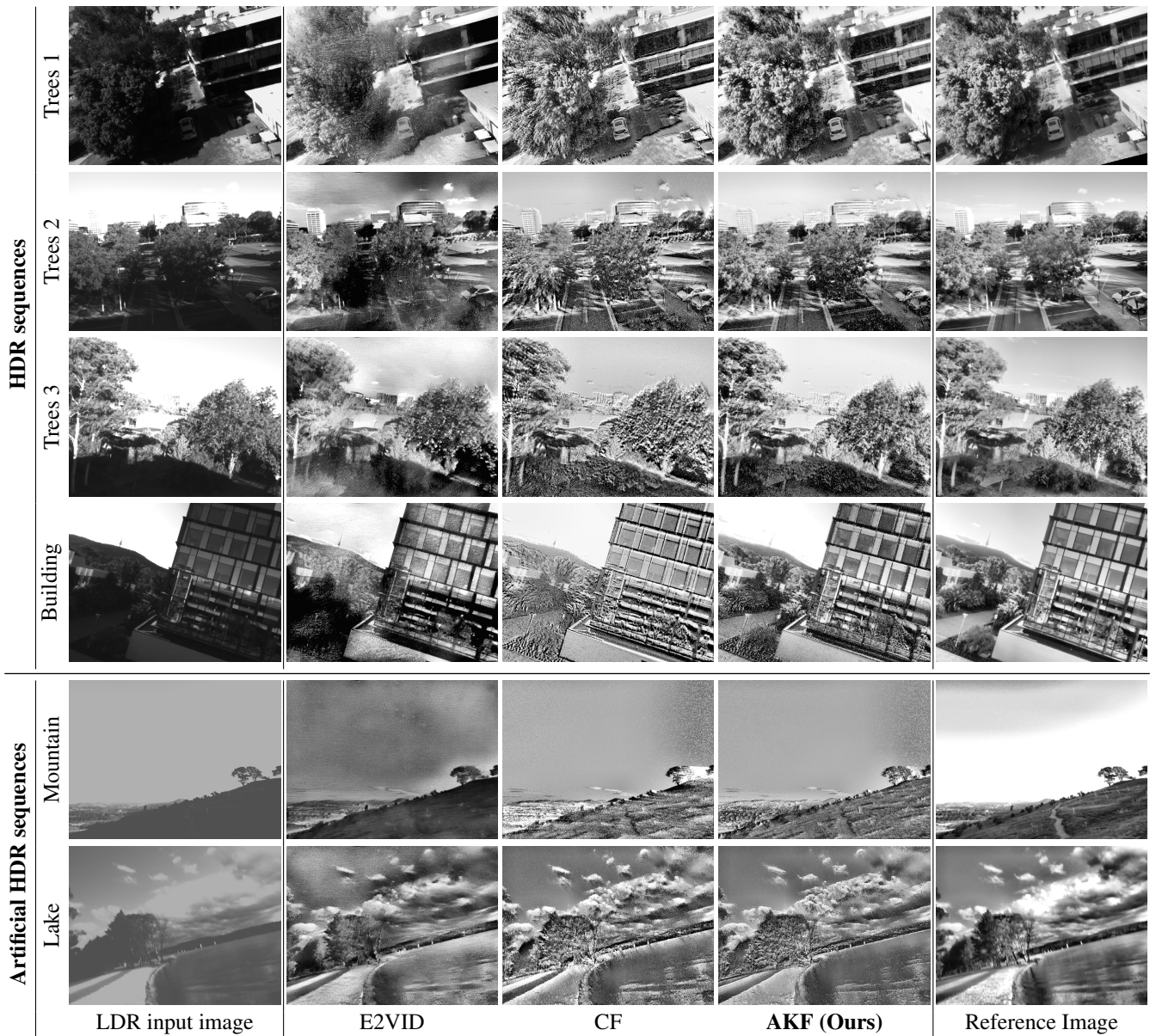


Figure 5: Results on our novel HDR dataset. E2VID [33] uses events only. The input images used in the CF and AKF are low dynamic range.

7 Conclusion

In this paper, we introduced an asynchronous Kalman-Bucy filter to reconstruct high frame rate HDR videos from LDR frames and event data. The Kalman gain is estimated pixel-by-pixel based on a unifying event/frame uncertainty model over time. To target HDR reconstruction, we presented a real-world, hybrid event/frame dataset captured on registered frame and event cameras. Our method outperformed the state-of-the-art event-based reconstruction methods on publicly available datasets and our HDR hybrid event/frame dataset. We believe our asynchronous Kalman filter has practical applications for video acquisition in HDR scenarios using the extended power of event cameras in addition to conventional frame-based cameras.

References

- [1] Patrick Bardow, Andrew J. Davison, and Stefan Leutenegger. Simultaneous optical flow and intensity estimation from an event camera. In *IEEE Conf. Comput. Vis. Pattern Recog. (CVPR)*, pages 884–892, 2016.
- [2] Herbert Bay, Tinne Tuytelaars, and Luc Van Gool. Surf: Speeded up robust features. In *European conference on computer vision*, pages 404–417. Springer, 2006.
- [3] Christian Brandli, Raphael Berner, Minhao Yang, Shih-Chii Liu, and Tobi Delbruck. A 240×180 130 db 3 μ s latency global shutter spatiotemporal vision sensor. *IEEE Journal of Solid-State Circuits*, 49(10):2333–2341, 2014.
- [4] Christian Brandli, Lorenz Muller, and Tobi Delbruck. Real-time, high-speed video decompression using a frame-and event-based davis sensor. In *2014 IEEE International Symposium on Circuits and Systems (ISCAS)*, pages 686–689. IEEE, 2014.
- [5] Shoushun Chen and Menghan Guo. Live demonstration: CeleX-V: A 1M pixel multi-mode event-based sensor. In *IEEE Conf. Comput. Vis. Pattern Recog. Workshops (CVPRW)*, 2019.
- [6] Matthew Cook, Luca Gugelmann, Florian Jug, Christoph Krautz, and Angelika Steger. Interacting maps for fast visual interpretation. In *Int. Joint Conf. Neural Netw. (IJCNN)*, pages 770–776, 2011.
- [7] Paul E Debevec and Jitendra Malik. Recovering high dynamic range radiance maps from photographs. In *ACM SIGGRAPH 2008 classes*, pages 1–10. 2008.
- [8] Tobi Delbruck. Frame-free dynamic digital vision. In *Proceedings of Intl. Symp. on Secure-Life Electronics, Advanced Electronics for Quality Life and Society*, pages 21–26. Citeseer, 2008.
- [9] Guillermo Gallego, Tobi Delbruck, Garrick Orchard, Chiara Bartolozzi, Brian Taba, Andrea Censi, Stefan Leutenegger, Andrew Davison, Jörg Conradt, Kostas Daniilidis, et al. Event-based vision: A survey. *arXiv preprint arXiv:1904.08405*, 2019.
- [10] Michael D Grossberg and Shree K Nayar. What is the space of camera response functions? In *2003 IEEE Computer Society Conference on Computer Vision and Pattern Recognition, 2003. Proceedings.*, volume 2, pages II–602. IEEE, 2003.
- [11] Jin Han, Chu Zhou, Peiqi Duan, Yehui Tang, Chang Xu, Chao Xu, Tiejun Huang, and Boxin Shi. Neuromorphic camera guided high dynamic range imaging. In *Proceedings of the IEEE/CVF Conference on Computer Vision and Pattern Recognition*, pages 1730–1739, 2020.
- [12] Janne Heikkila and Olli Silven. A four-step camera calibration procedure with implicit image correction. In *Proceedings of IEEE Computer Society Conference on Computer Vision and Pattern Recognition*, pages 1106–1112. IEEE, 1997.
- [13] Zhe Jiang, Yu Zhang, Dongqing Zou, Jimmy Ren, Jiancheng Lv, and Yebin Liu. Learning event-based motion deblurring. In *IEEE Conf. Comput. Vis. Pattern Recog. (CVPR)*, pages 3320–3329, 2020.
- [14] Rudolph Emil Kalman. A new approach to linear filtering and prediction problems. *Journal of basic Engineering*, 82(1):35–45, 1960.
- [15] Rudolph E Kalman and Richard S Bucy. New results in linear filtering and prediction theory. *Journal of basic engineering*, 83(1):95–108, 1961.
- [16] Hanme Kim, Ankur Handa, Ryad Benosman, Sio-Hoi Ieng, and Andrew J. Davison. Simultaneous mosaicing and tracking with an event camera. In *British Mach. Vis. Conf. (BMVC)*, 2014.
- [17] Hanme Kim, Stefan Leutenegger, and Andrew J. Davison. Real-time 3D reconstruction and 6-DoF tracking with an event camera. In *Eur. Conf. Comput. Vis. (ECCV)*, pages 349–364, 2016.
- [18] Min H Kim and Jan Kautz. Characterization for high dynamic range imaging. In *Computer Graphics Forum*, volume 27, pages 691–697. Wiley Online Library, 2008.
- [19] Patrick Lichtsteiner, Christoph Posch, and Tobi Delbruck. 128×128 120 dB 15 μ s latency asynchronous temporal contrast vision sensor. *IEEE journal of solid-state circuits*, 43(2):566–576, 2008.
- [20] Songnan Lin, Jiawei Zhang, Jinshan Pan, Zhe Jiang, Dongqing Zou, Yongtian Wang, Jing Chen, Zhe Jiang, and Jimmy Ren. Learning event-driven video deblurring and interpolation. In *Eur. Conf. Comput. Vis. (ECCV)*, volume 3, 2020.
- [21] Han-Chao Liu, Fang-Lue Zhang, David Marshall, Luping Shi, and Shi-Min Hu. High-speed video generation with an event camera. *The Visual Computer*, 33(6-8):749–759, June 2017.
- [22] Brian C Madden. Extended intensity range imaging. *Technical Reports (CIS)*, page 248, 1993.
- [23] Steve Mann. Comparametric equations with practical applications in quantigraphic image processing. *IEEE transactions on image processing*, 9(8):1389–1406, 2000.
- [24] Elias Mueggler, Henri Rebecq, Guillermo Gallego, Tobi Delbruck, and Davide Scaramuzza. The event-camera dataset and simulator: Event-based data for pose estimation, visual odometry, and SLAM. *Int. J. Robot. Research*, 36(2):142–149, 2017.
- [25] Manish Narwaria, Rafal Mantiuk, Mattheiu P Da Silva, and Patrick Le Callet. Hdr-vdp-2.2: a calibrated method for objective quality prediction of high-dynamic range and standard images. *Journal of Electronic Imaging*, 24(1):010501, 2015.
- [26] Liyuan Pan, Richard I. Hartley, Cedric Scheerlinck, Miaomiao Liu, Xin Yu, and Yuchao Dai. High frame rate video reconstruction based on an event camera. *IEEE Trans. Pattern Anal. Mach. Intell.*, 2020.
- [27] Liyuan Pan, Cedric Scheerlinck, Xin Yu, Richard Hartley, Miaomiao Liu, and Yuchao Dai. Bringing a blurry frame alive at high frame-rate with an event camera. In *Proceedings of the IEEE Conference on Computer Vision and Pattern Recognition*, pages 6820–6829, 2019.
- [28] Stefano Pini, Guido Borghi, Roberto Vezzani, and Rita Cucchiara. Video synthesis from intensity and event frames. In *International Conference on Image Analysis and Processing*, pages 313–323. Springer, 2019.
- [29] Stefano Pini, Guido Borghi, Roberto Vezzani, Rita Cucchiara University of Modena, and Reggio Emilia. Learn to see by events: Color frame synthesis from event and RGB cameras. *Int. Joint Conf. Comput. Vis., Image and Comput. Graph. Theory and Appl.*, 2020.
- [30] Christoph Posch, Daniel Matolin, and Rainer Wohlgenannt. A qvga 143 db dynamic range frame-free pwm image sensor with lossless pixel-level video compression and time-domain cds. *IEEE Journal of Solid-State Circuits*, 46(1):259–275, 2010.
- [31] Henri Rebecq, Timo Horstschäfer, Guillermo Gallego, and Davide Scaramuzza. EVO: A geometric approach to event-based 6-DOF parallel tracking and mapping in real-time. *IEEE Robot. Autom. Lett.*, 2(2):593–600, 2017.

- [32] Henri Rebecq, René Ranftl, Vladlen Koltun, and Davide Scaramuzza. Events-to-video: Bringing modern computer vision to event cameras. In *IEEE Conf. Comput. Vis. Pattern Recog. (CVPR)*, 2019.
- [33] Henri Rebecq, René Ranftl, Vladlen Koltun, and Davide Scaramuzza. High speed and high dynamic range video with an event camera. *IEEE Trans. Pattern Anal. Mach. Intell.*, 2020.
- [34] Christian Reinbacher, Gottfried Graber, and Thomas Pock. Real-time intensity-image reconstruction for event cameras using manifold regularisation. In *British Mach. Vis. Conf. (BMVC)*, 2016.
- [35] Fabrizio Russo. A method for estimation and filtering of gaussian noise in images. *IEEE Transactions on Instrumentation and Measurement*, 52(4):1148–1154, 2003.
- [36] Cedric Scheerlinck, Nick Barnes, and Robert Mahony. Continuous-time intensity estimation using event cameras. In *Asian Conf. Comput. Vis. (ACCV)*, 2018.
- [37] Cedric Scheerlinck, Nick Barnes, and Robert Mahony. Asynchronous spatial image convolutions for event cameras. *IEEE Robot. Autom. Lett.*, 4(2):816–822, Apr. 2019.
- [38] Cedric Scheerlinck, Henri Rebecq, Daniel Gehrig, Nick Barnes, Robert Mahony, and Davide Scaramuzza. Fast image reconstruction with an event camera. In *IEEE Winter Conf. Appl. Comput. Vis. (WACV)*, 2020.
- [39] Prasan Shedligeri and Kaushik Mitra. Photorealistic image reconstruction from hybrid intensity and event-based sensor. *J. Electron. Imaging*, 28(06):1, Dec. 2019.
- [40] Dong-Hyuk Shin, Rae-Hong Park, Seungjoon Yang, and Jae-Han Jung. Block-based noise estimation using adaptive gaussian filtering. *IEEE Transactions on Consumer Electronics*, 51(1):218–226, 2005.
- [41] Timo Stoffregen, Cedric Scheerlinck, Davide Scaramuzza, Tom Drummond, Nick Barnes, Lindsay Kleeman, and Robert Mahony. Reducing the Sim-to-Real gap for event cameras. In *Eur. Conf. Comput. Vis. (ECCV)*, 2020.
- [42] Zhou Wang, Alan C. Bovik, Hamid R. Sheikh, and Eero P. Simoncelli. Image quality assessment: From error visibility to structural similarity. *IEEE Trans. Image Process.*, 13(4):600–612, Apr. 2004.
- [43] Zihao W Wang, Peiqi Duan, Oliver Cossairt, Aggelos Katsaggelos, Tiejun Huang, and Boxin Shi. Joint filtering of intensity images and neuromorphic events for high-resolution noise-robust imaging. In *Proceedings of the IEEE/CVF Conference on Computer Vision and Pattern Recognition*, pages 1609–1619, 2020.
- [44] Zihao W. Wang, Weixin Jiang, Aggelos Katsaggelos, and Oliver Cossairt. Event-driven video frame synthesis. In *Int. Conf. Comput. Vis. Workshops (ICCVW)*, 2019.
- [45] Minhao Yang, Shih-Chii Liu, and Tobi Delbruck. A dynamic vision sensor with 1% temporal contrast sensitivity and in-pixel asynchronous delta modulator for event encoding. *IEEE Journal of Solid-State Circuits*, 50(9):2149–2160, 2015.
- [46] Richard Zhang, Phillip Isola, Alexei A. Efros, Eli Shechtman, and Oliver Wang. The unreasonable effectiveness of deep features as a perceptual metric. In *IEEE Conf. Comput. Vis. Pattern Recog. (CVPR)*, 2018.
- [47] Zhengyou Zhang. A flexible new technique for camera calibration. *IEEE Transactions on pattern analysis and machine intelligence*, 22(11):1330–1334, 2000.
- [48] Alex Zihao Zhu, Dinesh Thakur, Tolga Ozaslan, Bernd Pfrommer, Vijay Kumar, and Kostas Daniilidis. The multivehicle stereo event camera dataset: An event camera dataset for 3D perception. *IEEE Robot. Autom. Lett.*, 3(3):2032–2039, July 2018.
- [49] Karel Zuiderveld. Contrast limited adaptive histogram equalization. *Graphics gems*, pages 474–485, 1994.

AN ASYNCHRONOUS KALMAN FILTER FOR HYBRID EVENT CAMERAS

SUPPLEMENTARY MATERIALS

1 Experimental Details

1.1 Our hybrid event/frame Datasets

The hybrid event/frame camera rig we built is shown in Figure 6. We use the camera rig to collect events, frames and HDR reference images. The details of our proposed HDR event/frame dataset are summarized in Table 3. The dataset sequences focus on different HDR scenes with different camera motion speeds, which is challenging for all event-based HDR image reconstruction methods. All datasets will be released after publication.

Hybrid event/frame system settings:

An external trigger signal from the RGB camera is sent through a signal amplifier to trigger timestamped zero magnitude events in the event camera for time synchronization (see Figure 6). The FLIR RGB frame camera captures RGB videos and the Prophesee event camera captures the event streams. For our HDR dataset, the reference HDR image is generated from several low dynamic range raw images taken by the RGB camera at different exposures, and fused using the MATLAB `makehdr` command.

For our AHDR dataset, we apply an artificial camera response function to RGB camera output frames to simulate a low dynamic range camera (see Figure 7). Following the process introduced in the main paper §3.2.1, we experimentally determine the corresponding camera uncertainty function of the low dynamic range camera (see Figure 8). The resulting image noise covariance is high for the ‘cropped’ intensity values.

More results:

In addition to the results presented in the main paper, we demonstrate more qualitative comparison in Figure 9. E2VID and ECNN reconstruct the trees and buildings correctly, but exhibit many undesirable artifacts in areas with sparse or noisy events *e.g.*, skies. Interestingly, E2VID and ECNN perform poorly on the bottom left corner in Figure 9 (b) and (c), because the centre of camera rotation has less events occurring. On the other hand, the cutoff frequency of CF, which corresponds to the Kalman gain of our AKF is a single constant value for all pixels. Hence, the CF results always exhibit ‘bleeding’ effect on object edges. AKF overcomes this by dynamically adjusting the per-pixel Kalman gain according to events and frame uncertainty model.

We demonstrate the quantitative results of ECNN in the main paper and the qualitative images are shown in Figure 10. ECNN achieves good reconstructions on indoor, less noisy IJRR datasets (Figure 11 and 12), but performs poorly on our challenging dataset. As previously discussed, it is sensitive to noisy events, *e.g.*, hot pixels in the sky of Figure 10 (e) and (f). Areas with less events near the camera rotation centre are wrongly reconstructed in Figure 10 (a)-(d).

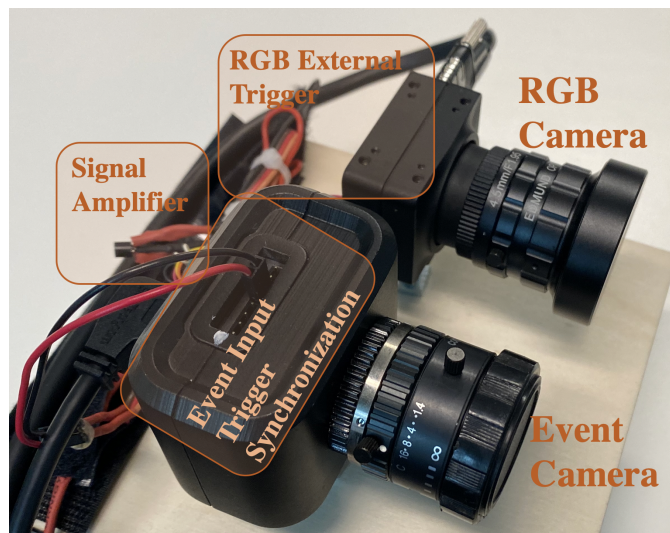


Figure 6: Our Hybrid event/frame System

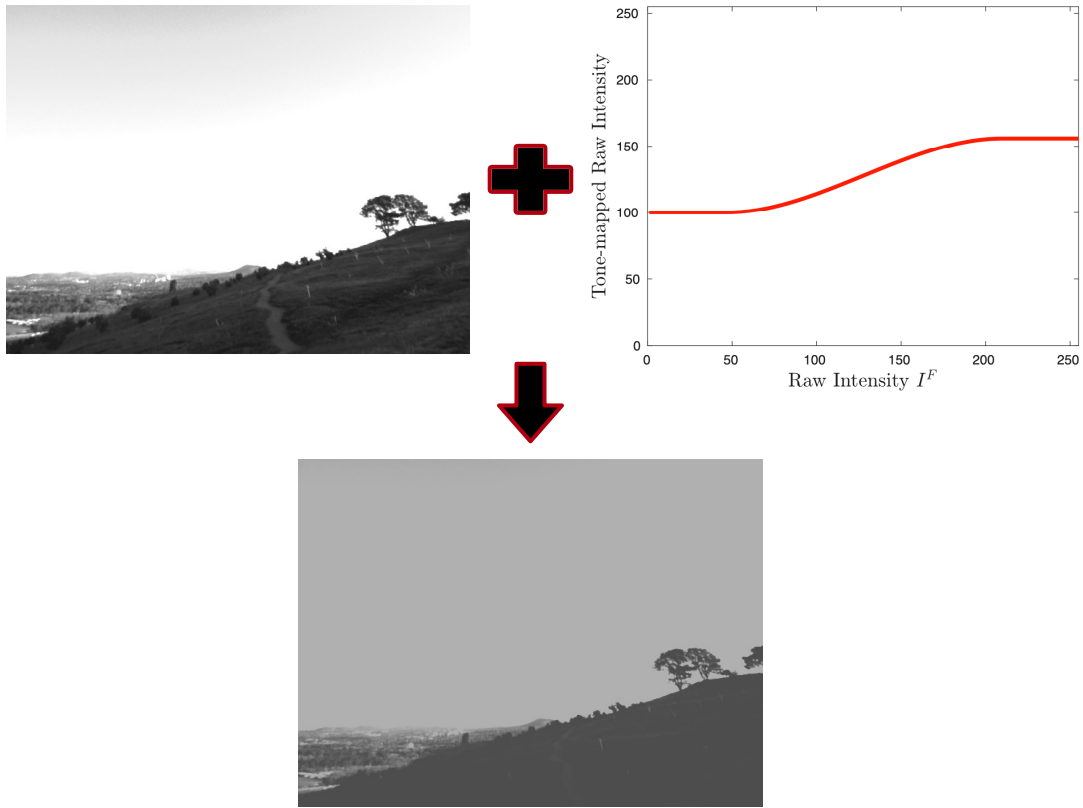


Figure 7: Process of generating our AHDR dataset. We simulate a low dynamic range camera by applying an artificial camera response function to real images.

HDR Dataset	# of images	Speed	Description	HDR Scene	Reference Image
HDR sequences					
city	150	medium	rooftop overlooking city buildings	dark buildings	✓
trees 1	208	slow and fast	a car under tree shadow	tree shadow	✓
trees 2	150	medium	parking lot, buildings and clouds	bright far-away buildings	✓
trees 3	150	medium	trees partially covered by shadow and far away buildings	buildings and shadow	✓
building	150	medium	mountain, tower, building and plants	dark plants	✓
Artificial HDR sequences (AHDR)					
mountain	150	slow and fast	mountain with road overlooking city	dark grass and road	✓
lake	200	slow and fast	side of lake with trees and road during cloudy day	trees and clouds	✓

Table 3: Details of our proposed HDR event/frame dataset.

1.2 IJRR Datasets

In the main paper, we demonstrate the mean qualitative results on IJRR [24] DAVIS event camera dataset. We provide the detailed qualitative results in Table 5 and qualitative samples in Figure 11 and 12. Because many of the image sequences in IJRR are dark, we increase contrast of all results and reference images using adaptive histogram equalization (CLAHE) [49] for better visualization.

Results of the deep-learning based reconstruction methods (E2VID and ECNN) correctly recover the structure of scenes but all output images are washed-out even after applying histogram equalization. It is difficult to estimate correct intensity range without image fusion. Also, E2VID and ECNN are sensitive to noisy events *e.g.*, hot pixels in Figure 11 (d) on top left corner. The event/frame reconstruction method (CF) achieves correct intensity range but suffers from double edges effect due to the zero-order-hold assumption that disregards intensity changes between frames. Our AKF overcomes the limitation of low frame rate input intensities by frame interpolation and augmentation. It performs the best among the four methods.

Algorithm 1 Event-based Continuous-time Intensity Estimation Using Asynchronous Kalman Filter

```

1: Initialise variables
2: for New  $i^{\text{th}}$  event at pixel  $\vec{p}$ ,  $e(t_{\vec{p}}^i)$  do
3:   if new image frame arrives then
4:     Deblur new image based on [27]
5:     Compute  $c(\tau^k)$  based on Eq (10)
6:   end if
7:   Update augmented frame  $\hat{L}_{\vec{p}}^A(t_{\vec{p}}^i)$  based on Eq (8)- (11)
8:   Update image covariance  $R_{\vec{p}}(t_{\vec{p}}^i)$  based on Eq (4)- (7)
9:   Update state  $\hat{L}_{\vec{p}}(t_{\vec{p}}^i)$  based on Eq (14)-(16)
10:  Update covariance  $P_{\vec{p}}(t_{\vec{p}}^i)$  based on Eq (18)-(19), where  $Q$  is designed based on discussions in §3.1
11:  if publishing new image then
12:    for all pixels  $\vec{q}$  do
13:      Update state  $\hat{L}_{\vec{q}}(t_{\vec{q}}^i)$  based on Eq (16)
14:      Update covariance  $P_{\vec{q}}(t_{\vec{q}}^i)$  based on Eq (18)-(19), where  $Q$  corresponds to zero event covariance
15:      Write image
16:    end for
17:  end if
18: end for

```

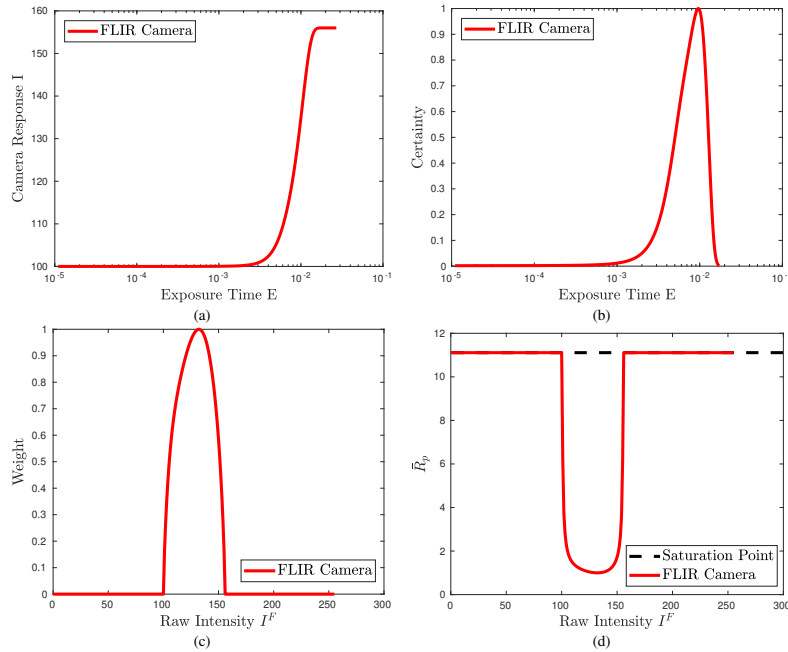


Figure 8: Simulated low dynamic range camera functions for the FLIR camera used in the AHDR datasets.

2 Abbreviations and Notations

3 High Frame Rate Videos

Our AKF continuously updates image state as events arrive. Reconstructed images can be generated at any event time allowing construction of a video with frame rate as high as the event rate. In our supplementary videos, we generate high frame rate (output 1500Hz shown in slow motion), HDR reconstructed videos to demonstrate our continuous-time intensity reconstruction.

Due to the use of greyscale event camera, only luminance changes can be captured, we evaluate our results primarily on greyscale video reconstruction. In the supplementary videos, we show preliminary results for color output by acquiring chrominance components from the input color frames and applying these to the reconstructed grayscale luminance. However, the proposed algorithm is also applicable for color event streams, where each channel could be processed independently to produce color videos.



Figure 9: Comparison of the state-of-the-art methods of event-based video reconstruction on trees (a-f) and city (g-l) dataset. E2VID and ECNN are neural networks that use only events to reconstruct video. CF and AKF are continuous-time filters that fuse events and frames.

Notations	Keys
AKF	Asynchronous Kalman Filter
CF	Complementary filter [36]
ECNN	Event camera neural network [41]
E2VID	Event-to-Video [33]
EDI	Event double integral [27]
HDR	High dynamic range
AHDR	Artificial high dynamic range
CRF	Camera response function
e	Event
c	Event contrast threshold
I	Sensor response
I^F	Raw intensity frame
L^F	Log intensity frame
L^A	Augmentated log intensity frame
P	State noise covariance
Q	Event noise covariance
R	Image noise covariance
K	Kalman gain

Table 4: Key abbreviations and notations.

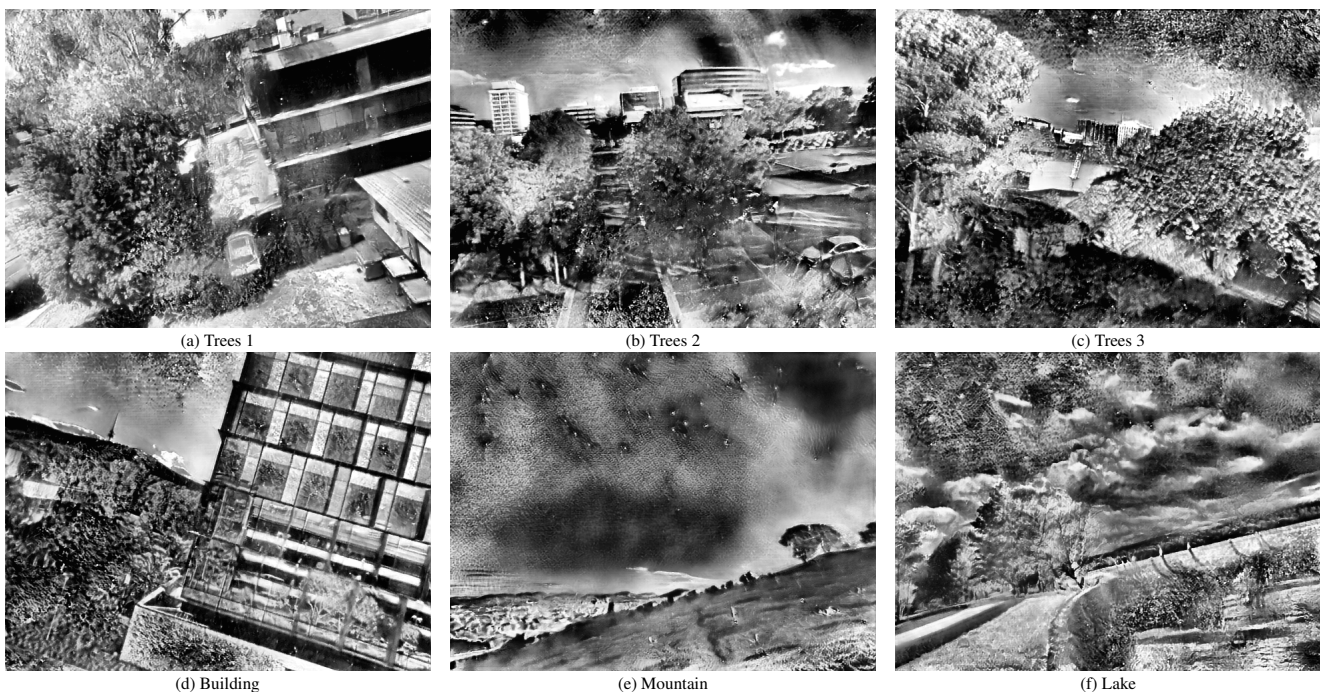


Figure 10: ECNN [41] results on our novel HDR dataset (Fig a-d) and our AHDR dataset (Fig e and f).

Metrics	MSE ($\times 10^{-2}$) \downarrow				SSIM \uparrow				LPIPS \downarrow			
Methods	E2VID	ECNN	CF	AKF (ours)	E2VID	ECNN	CF	AKF (ours)	E2VID	ECNN	CF	AKF (ours)
boxes_6dof	11.87	3.99	0.33	0.26	0.51	0.62	0.78	0.80	0.34	0.24	0.26	0.26
calibration	23.46	3.05	0.11	0.09	0.43	0.65	0.92	0.92	0.31	0.18	0.09	0.07
dynamic_6dof	30.96	14.11	0.13	0.12	0.24	0.30	0.88	0.87	0.46	0.36	0.18	0.20
office_zizang	17.14	3.95	0.26	0.22	0.40	0.49	0.85	0.86	0.40	0.25	0.22	0.22
poster_6dof	21.68	6.86	0.29	0.26	0.34	0.46	0.78	0.79	0.35	0.22	0.22	0.24
shapes_6dof	19.44	8.77	0.16	0.11	0.68	0.76	0.92	0.94	0.31	0.18	0.16	0.15
slider_depth	20.13	4.16	0.21	0.18	0.44	0.61	0.83	0.86	0.40	0.23	0.22	0.21
Mean	20.67	6.41	0.21	0.18	0.43	0.56	0.85	0.86	0.37	0.24	0.19	0.19

Table 5: Comparison of the state-of-the-art methods of event-based video reconstruction on IJRR [24] DAVIS datasets.

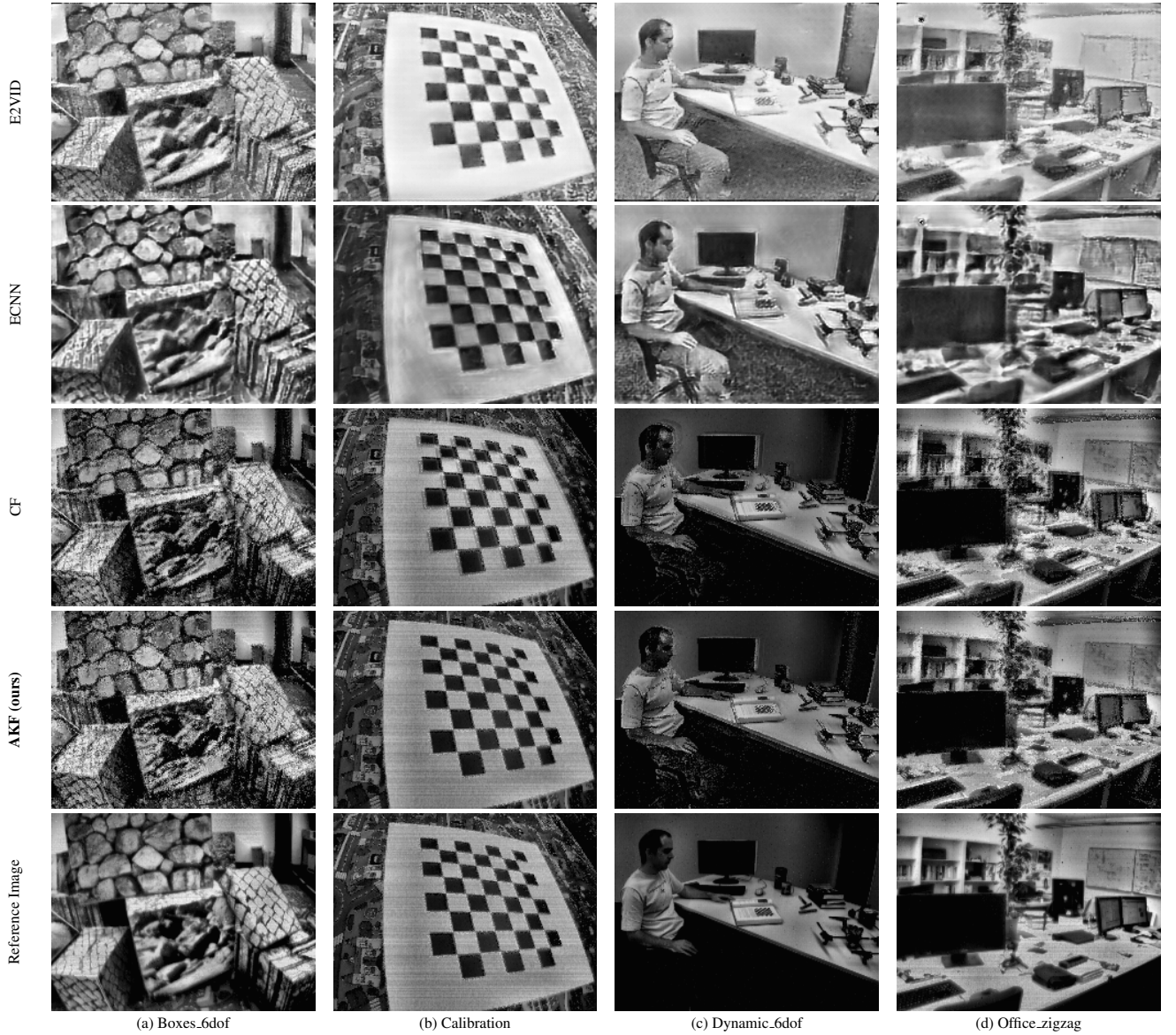


Figure 11: Comparison of the state-of-the-art methods of event-based video reconstruction on IJRR [24] Dataset

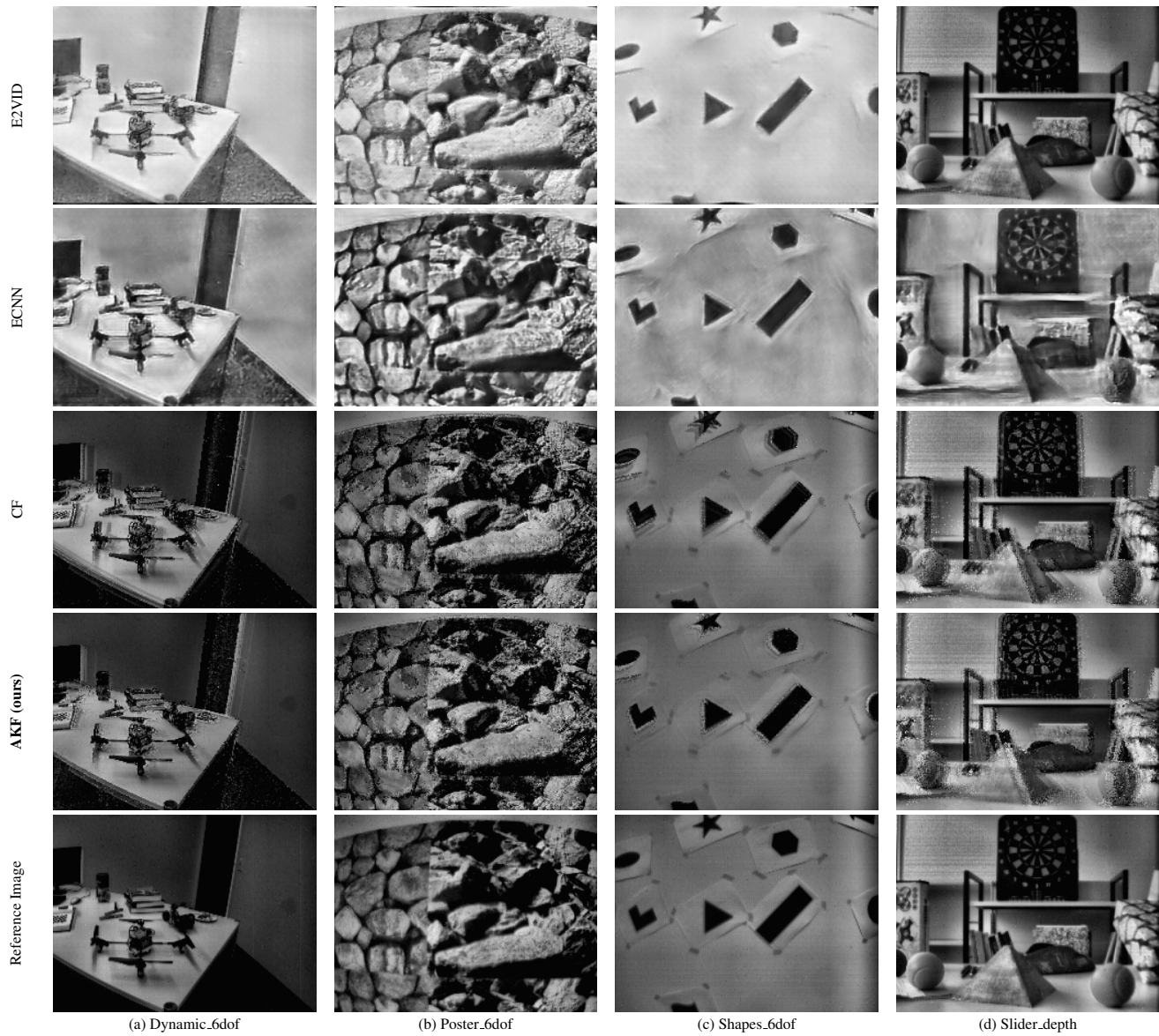


Figure 12: Comparison of the state-of-the-art methods of event-based video reconstruction on IJRR [24] Dataset

4 Derivation of $P_{\bar{p}}(t)$

Within a time-interval $t \in [t_{\bar{p}}^i, t_{\bar{p}}^{i+1})$, the ODE of $P_{\bar{p}}(t)$ is

$$\frac{1}{P_{\bar{p}}^2(t)} \frac{dP_{\bar{p}}(t)}{dt} = -R_{\bar{p}}^{-1}(t).$$

Moving dt to the right hand side yields

$$\frac{1}{P_{\bar{p}}^2(t)} dP_{\bar{p}}(t) = -R_{\bar{p}}^{-1}(t) dt.$$

Integrate from event time $t_{\bar{p}}^i$ to time t

$$\begin{aligned} \int_{t_{\bar{p}}^i}^t \frac{1}{P_{\bar{p}}^2(t)} dP_{\bar{p}}(t) &= \int_{t_{\bar{p}}^i}^t -R_{\bar{p}}^{-1}(t) d\gamma, \\ -P_{\bar{p}}^{-1}(t) &= -R_{\bar{p}}^{-1}(t) \cdot (t - t_{\bar{p}}^i) + C_1, \\ P_{\bar{p}}(t) &= \frac{1}{R_{\bar{p}}^{-1}(t) \cdot (t - t_{\bar{p}}^i) - C_1}, \end{aligned}$$

where C_1 is a constant number.

Let $t = t_{\bar{p}}^i$ and we have

$$\begin{aligned} P(t_{\bar{p}}^i) &= \frac{1}{-C_1}, \\ C_1 &= -P_{\bar{p}}^{-1}(t_{\bar{p}}^i). \end{aligned}$$

The solution of the ODE of $P_{\bar{p}}(t)$ is

$$P_{\bar{p}}(t) = \frac{1}{P_{\bar{p}}^{-1}(t_{\bar{p}}^i) + R_{\bar{p}}^{-1}(t) \cdot (t - t_{\bar{p}}^i)}.$$

5 Derivation of $\hat{L}_{\bar{p}}(t)$

Within a time-interval $t \in [t_{\bar{p}}^i, t_{\bar{p}}^{i+1})$, the ODE of $\hat{L}_{\bar{p}}(t)$ is

$$\begin{aligned} \dot{\hat{L}}_{\bar{p}}(t) &= -\frac{R_{\bar{p}}^{-1}(t) \cdot [\hat{L}_{\bar{p}}(t) - L_{\bar{p}}^A(t)]}{P_{\bar{p}}^{-1}(t_{\bar{p}}^i) + R_{\bar{p}}^{-1}(t) \cdot (t - t_{\bar{p}}^i)}, \\ \frac{d[\hat{L}_{\bar{p}}(t) - L_{\bar{p}}^A(t)]}{\hat{L}_{\bar{p}}(t) - L_{\bar{p}}^A(t)} &= -\frac{R_{\bar{p}}^{-1}(t)}{P_{\bar{p}}^{-1}(t_{\bar{p}}^i) + R_{\bar{p}}^{-1}(t) \cdot (t - t_{\bar{p}}^i)} dt. \end{aligned}$$

Integrate from the event time $t_{\bar{p}}^i$ to time t

$$\begin{aligned} &\ln(\hat{L}_{\bar{p}}(t) - L_{\bar{p}}^A(t)) \\ &= \int_{t_{\bar{p}}^i}^t -\frac{R_{\bar{p}}^{-1}(t)}{P_{\bar{p}}^{-1}(t_{\bar{p}}^i) + R_{\bar{p}}^{-1}(t) \cdot (\gamma - t_{\bar{p}}^i)} d\gamma \\ &= -\ln(P_{\bar{p}}^{-1}(t_{\bar{p}}^i) + R_{\bar{p}}^{-1}(t) \cdot (t - t_{\bar{p}}^i)) + C_2, \end{aligned}$$

where C_2 is a constant number. Take exponential of both sides

$$\hat{L}_{\bar{p}}(t) - L_{\bar{p}}^A(t) = \frac{1}{P_{\bar{p}}^{-1}(t_{\bar{p}}^i) + R_{\bar{p}}^{-1}(t) \cdot (t - t_{\bar{p}}^i)} \cdot e^{C_2},$$

and we define $C_3 = e^{C_2}$.

Let $t = t_{\vec{p}}^i$ and we have

$$\begin{aligned}\hat{L}_{\vec{p}}(t_{\vec{p}}^i) - L_{\vec{p}}^A(t_{\vec{p}}^i) &= \frac{1}{P_{\vec{p}}^{-1}(t_{\vec{p}}^i)} \cdot C_3, \\ C_3 &= [\hat{L}_{\vec{p}}(t_{\vec{p}}^i) - L_{\vec{p}}^A(t_{\vec{p}}^i)] \cdot P_{\vec{p}}^{-1}(t_{\vec{p}}^i).\end{aligned}$$

The solution of the ODE of $\hat{L}_{\vec{p}}(t)$ is

$$s\hat{L}_{\vec{p}}(t) = \frac{[\hat{L}_{\vec{p}}(t_{\vec{p}}^i) - L_{\vec{p}}^A(t_{\vec{p}}^i)] \cdot P_{\vec{p}}^{-1}(t_{\vec{p}}^i)}{P_{\vec{p}}^{-1}(t_{\vec{p}}^i) + R_{\vec{p}}^{-1}(t) \cdot (t - t_{\vec{p}}^i)} + L_{\vec{p}}^A(t).$$